Quantum Mechanical Calculations of Tryptophan and Comparison with Conformations in Native Proteins

ARTICLE *in* THE JOURNAL OF PHYSICAL CHEMISTRY A · JANUARY 2007

Impact Factor: 2.69 · DOI: 10.1021/jp062921n · Source: PubMed

3 AUTHORS:

Ersin Yurtsever
Koc University
138 PUBLICATIONS **1,227** CITATIONS
SEE PROFILE

Deniz Yuret
Koc University
66 PUBLICATIONS **1,229** CITATIONS
SEE PROFILE

Burak Erman
Koc University
220 PUBLICATIONS **5,940** CITATIONS
SEE PROFILE

Quantum Mechanical Calculations of Tryptophan and Comparison with Conformations in Native Proteins

Ersin Yurtsever,*,† Deniz Yuret,‡ and Burak Erman‡

College of Arts and Sciences and College of Engineering, Koc University, Rumelifeneri Yolu, Sariyer 34450 Istanbul, Turkey

Received: May 12, 2006; In Final Form: October 16, 2006

We report a detailed analysis of the potential energy surface of *N*-acetyl-L-tryptophan-*N*-methylamide, (NATMA) both in the gas phase and in solution. The minima are identified using the density-functional-theory (DFT) with the 6-31g(d) basis set. The full potential energy surface in terms of torsional angles is spanned starting from various initial configurations. We were able to locate 77 distinct L-minima. The calculated energy maps correspond to the intrinsic conformational propensities of the individual NATMA molecule. We show that these conformations are essentially similar to the conformations of tryptophan in native proteins. For this reason, we compare the results of DFT calculations in the gas and solution phases with native state conformations of tryptophan obtained from a protein library. In native proteins, tryptophan conformations have strong preferences for the β sheet, right-handed helix, tight turn, and bridge structures. The conformations calculated by DFT, the solution-phase results in particular, for the single tryptophan residue are in agreement with native state values obtained from the Protein Data Bank.

Introduction

Important events along electron-transfer pathways, such as in photosynthesis and respiration, for example, are controlled predominantly by the amino acid tryptophan (Trp).[1] Activity and function of Trp is strongly dependent on the local configurations of the protein in the native state. For this reason, a detailed understanding of the conformational preferences is of importance, and indeed, it has been studied widely in recent years. Infrared and ultraviolet spectra of *N*-acetyltryptophan methylamide and comparison with results of density functional theory (DFT)[2] calculations indicate two dominant low energy conformers, C5, with its extended dipeptide backbone, or C7, in which the dipeptide backbone forms a seven-membered ring joined by an H bond between the C-amide NH and the ϕ-amide carbonyl groups. Huang and Lin[3] performed an extensive ab initio conformational search to characterize the gas-phase structures of tryptophan. They obtained 45 local minima. The minimum energy conformation among these accounted for 48.6% of all the conformations at equilibrium at 298 K. This is consistent with experimental results.[4] Bombasaro et al.,[5] determined the potential energy surface (PES) using ab initio and DFT calculations and obtained a total of 34 or 35 minimum energy conformations, depending on the method they used. They also verified that the C7 and C5 were the lowest energy conformations. In the present work, we report a more detailed analysis of *N*-acetyl-L-tryptophan-*N*-methylamide, (NATMA) both in the gas phase and in solution.

The state of a residue in the absence of neighboring residues indicates the intrinsic propensity or the backbone preference of that residue to be in that state. In this respect, the previous[2,3,5] and the present quantum mechanical analyses of NATMA yield its intrinsic propensities. If the residue is embedded in the polypeptide chain, its states may be correlated with those of the neighboring residues (local correlations) along the chain and those distant along the chain (long-range correlations). Other residues may occupy the immediate environment of a residue, such as in the compact internal regions of a native conformation, or it may be in interaction with the aqueous environment. The same residue may be inside or on the surface in contact with water, depending on the type of the protein. Thus, it is important to study a residue in both environments.

A precise determination of the intrinsic propensity of a residue is important because it serves as the reference state above which other interactions add. The intrinsic propensities of a single residue, X, may suitably be calculated by adopting a methyl capped dipeptide by inserting the residue X into *N*-acetyl-*N*′-methylamide to form Ace-X-Nme.[6−10] Recent calculations and measurements of NMR coupling constants give insights into intrinsic backbone preferences in dipeptides and longer sequences.[10] Calculations on tripeptides, Ace-X_1-X_2-Nme, or longer sequences show that the conformational states of neighboring residues are correlated[8,11,12] due to near neighbor (NN) effects. The electrostatic screening model[13] explains why the ϕ angles of a residue, for example, are shifted toward more negative values if the neighboring residues of a given residue X are aromatic or β-branched. An alternative explanation is the formation of hydrogen bonds between side chains and the backbone for sequences longer than dipeptides.[14,15] The electrostatic screening model describes the residue in aqueous medium; the hydrogen bond model does not. Understanding the behavior of a residue in the presence and absence of water is important to distinguish between different models.

The plan of the paper is as follows: In Section 2, we explain the computational tools used in the present work. In Section 3 we present the results obtained on NATMA, followed by a discussion of results in Section 4, where the computed calculations of NATMA are compared in detail with conformations of the tryptophan residue in native proteins.

* To whom correspondence should be addressed.
† College of Arts and Sciences.
‡ College of Engineering.

10.1021/jp062921n CCC: $33.50
Published on Web 12/01/2006

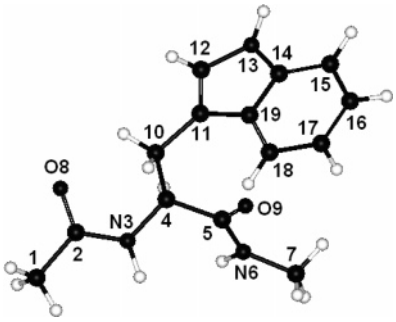

Figure 1. The geometry and labeling of NATMA.

2. Computational Methods

The PES of *N*-acetyl-L-tryptophan-*N*-methylamide has been studied in detail in the gas-phase using Gaussian03 program, version B.05.[16] The minima have been calculated from the density-functional-theory (DFT) calculations using the 6-31g-(d) basis set. The three-parameter-hybrid functional of Becke[17] is chosen as this combination of the basis set, and the functional has been numerously shown to produce reliable structures and energy values for organic molecules. In Figure 1, the basic structure and numbering of atoms along the backbone as well as the indole ring is given. For amino acids, the optimum points along the PES are usually characterized by the ranges of several torsional angles, such as in Ramachandran plots. The relevant torsional angles for our study are defined through four atoms and they are φ (2-3-4-10), ψ (3-4-5-6), χ_1 (3-4-10-11), χ_2 (4-10-11-12), ω_0 (1-2-3-4), and ω_1 (4-5-6-7).

The PES in terms of torsional angles is spanned by two different strategies and minima are located. First, we have generated a large number of starting configurations by restricting torsional angles to all possible permutations of sp^3 or sp^2 hybridizations. For example χ_2 (4-10-11-12) is chosen either as 0° or ±120°. There are six torsional combinations of atoms bonded to C_α (atoms N3, C5 and H). Similarly, for each set of bonds originating from C5, N3, C2 and N6, there are two permutational isomers. All possible combinations of these restrictions result in $3 \times 6 \times 2^4 = 288$ configurations. These starting configurations are then optimized by 6-31 g(d) basis set and those which result in D structures are discarded. In this manner, we were able to locate 62 distinct L-minima. To such generated structures, we have added 34 structures reported by Bombasaro et al.,[5] and we have discarded the duplicate structures. The final list contains 77 distinct minima that serve as a complete descriptor of the PES.

3. Results

We have plotted the distribution of four essential torsional angles in Figure 2 to summarize the structural variations of L-Trp. In this plot, the relative energies of these minima are not taken into account. That is, a structure is included even though its population at relatively high temperatures is negligible. The general characteristics of these plots show that Φ has a bimodal distribution located at $-175° < \varphi < -60°$ and around 60° respectively. In contrast, angle ψ has a smooth variation covering a wide range from −180° to 180°. Two torsional angles defining the position of the indole ring with respect to the backbone shows an almost equal distribution of sp^3 isomers.

In order to select the minima that are accessible at room temperatures, we resort to calculations that are more accurate. Using the 6-31(d) optimized structures, we calculated single point energies again with B3LYP functionals and a much larger basis set of 6-311++(d,p) which contains polarization functions on hydrogens as well as diffuse functions so that long range interactions are treated more accurately. Figure 3 shows the correlation between energy values (relative to the global minima in kJ/mol) of these two sets. Even though the general agreement between these calculations seems to be reasonable, the magnitudes of energy differences, especially at low-energy regime can be quite different. Still, the predicted gas-phase global minimum is the same in both calculations ($\varphi = -82.3$, $\psi = 59.7$, $\chi_1 = 47.7$, $\chi_2 = 82.6$, $\omega_0 = -174.2$ and $\omega_1 = 179.4$) which was reported also in ref 3 as the global minimum.

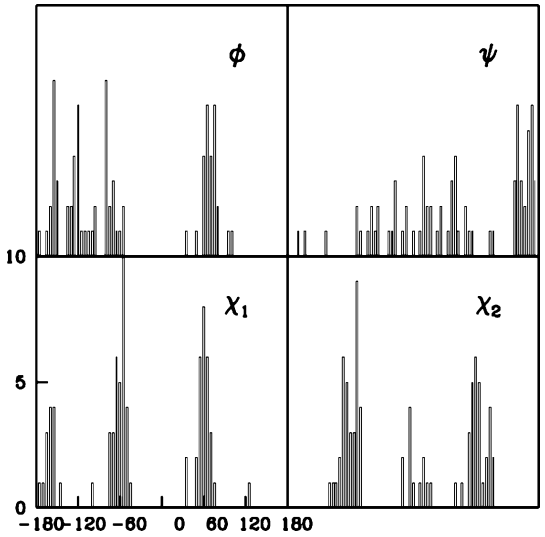

Figure 2. Histograms of torsion angles for all minima.

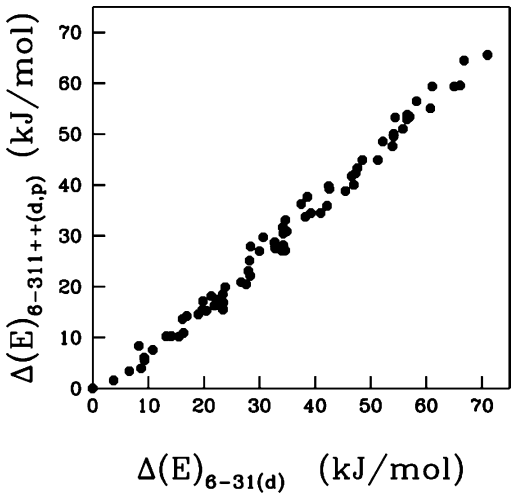

Figure 3. Comparison of the energy values obtained with the two basis sets.

The changes of the PES upon solvating tryptophan in water are studied by the polarized continuum model of Tomasi et.al[18−20] in which a cavity holding the solute molecule is defined by overlapping spheres. Then the solvent reaction field is written as a polarization charge density along the surface of this cavity. The free energy of solvation calculated in this manner within the PCM approach including the nonelectrostatic terms and the comparison between the gas-phase energy and the free energy (F) of solvation is presented in Figure 4, where the filled circles and the open squares are results from two different basis sets as indicated in the figure.

For both basis sets, the correlations between the gas phase and solvated energies are rather high for statistical purposes. However, the detailed energy differences, hence the populations

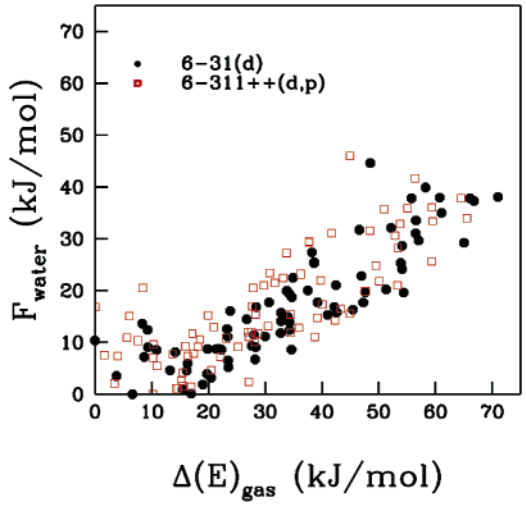

Figure 4. Comparison of the gas-phase energy and the free energy of solvation.

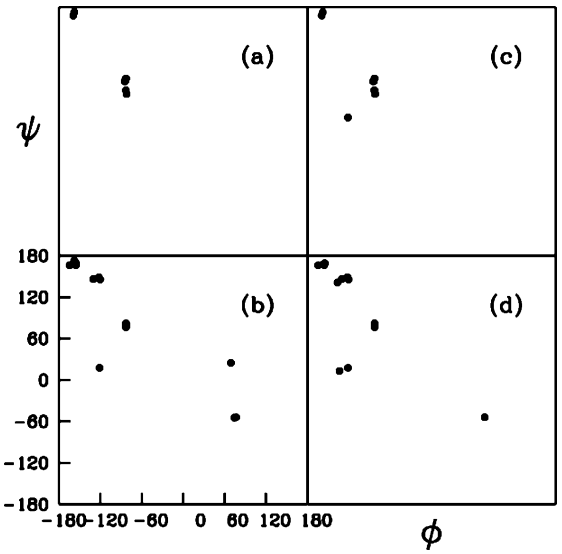

Figure 5. (a) Gas-phase energy with 6-31(d), (b) free energy of solvation with 6-31(d), (c) gas-phase energy with 6-311++(d, p), (d) free energy of solvation with 6-311++(d, p).

of the minima, are quite different. Both the quality of the basis set, especially the long-range behavior of the wavefunction, and the solvent effects seem to be very crucial to correlate computational results to the experimental ones. To illustrate this point, we plot the structures where the Boltzmann populations are above %1 at room temperature in Figure 5 in a Ramachandran plot of (φ, ψ).

Our earlier test runs with smaller basis sets have shown us that any basis smaller than 6-31(d) would give very poor results. The differences between two basis sets used here do not seem to be very significant in this plot, but they become more pronounced when less populated minima are included. On the other hand, the solvent effect is prominent for both basis sets.

A similar plot in (χ_1, χ_2) space is given in Figure 6.

In both basis sets, the gas-state populations are dominated by a single structure; however, for solvated L-Trp a large number of local minima have significant populations. In order to accentuate this difference, we present the actual populations of all minima in the following Figure 7. Here, the abscissa denotes the solvation energy of all 77 minima for the solution phase. The filled circles represent the Boltzmann population of these minima. The empty circles denote the populations of the 77

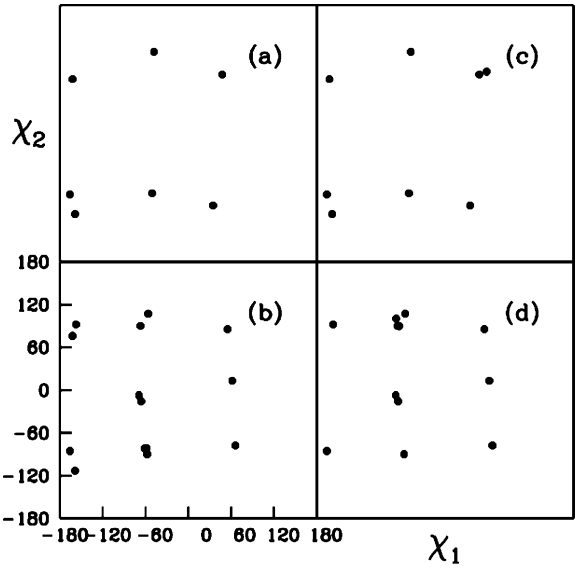

Figure 6. Parts a, b, c, and d represent the same calculations, respectively, as in Figure 5.

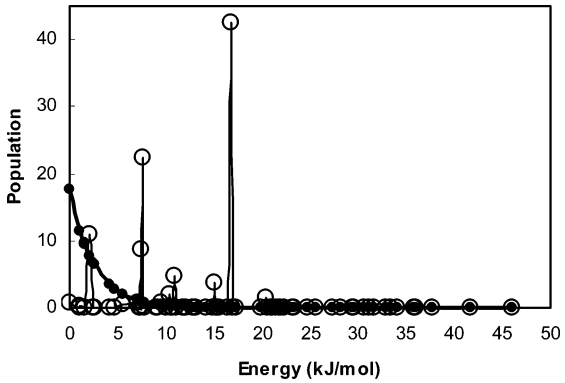

Figure 7. Boltzmann probability of all minima at room temperature. Filled circles correspond to the solvated molecule and open circles are the gas-phase results.

minima calculated for the gas phase. For each filled point of the solution phase there is a corresponding empty circle for the gas phase, and the corresponding populations are different. There is only one peak (at 2 kJ/mol) with relatively similar populations in both phases. This distribution clearly shows the necessity of including solvent effects in comparing theoretical results to the experimental data.

All minima which have room-temperature Boltzmann populations above %0.5 either for the gas or the solution case are listed in Table 1 with corresponding torsional angles. Boltzmann populations for the gas and solution phases presented in the penultimate and the last columns are calculated from:

$$P_j = \frac{e^{-\beta E(j)}}{\sum_i e^{-\beta E(i)}} \quad (1)$$

where $E(j)$ is the energy of the conformation in the gas phase or solution, $\beta = 1/kT$ and the summation index i runs overall conformations.

In order to detect the changes in the electronic structure upon solvation, we have calculated weighted average charges on each atom in the backbone as well as the indole ring. In the computation of these averages, each minimum is included in the summation weighed with its Boltzmann probability. The

TABLE 1: List of All Minima Boltzmann Populations above %0.5

no.	ϕ	ψ	χ_1	χ_2	P (gas)	P (solution)
1	−122	149	−69	−7	0.72	17.77
2	−155	169	66	−77	0.12	11.56
3	−164	166	55	85	0.14	11.39
4	−130	146	−58	−90	0.05	9.77
5	−120	146	−67	90	0.09	9.45
6	−83	77	−166	−85	10.89	7.73
7	−136	141	−65	90	0.00	6.72
8	−121	18	−66	−16	0.09	6.39
9	−155	166	62	13	0.09	3.36
10	−134	13	−69	100	0.01	2.67
11	77	−54	−56	107	0.54	1.96
12	−83	82	−157	92	0.70	1.02
13	75	19	−53	109	0.01	0.98
14	−159	168	−162	76	8.65	0.93
15	−122	14	−58	−84	0.06	0.91
16	−158	173	−159	−113	22.34	0.85
17	−81	−15	−56	112	0.07	0.44
18	−113	10	50	−99	0.68	0.39
19	−121	20	58	87	2.05	0.28
20	−84	73	−48	115	4.60	0.22
21	−84	72	−50	−84	3.71	0.04
22	−83	60	48	83	42.55	0.02
23	−82	54	35	−101	1.48	0.00

TABLE 2: Average Charge on Different Backbone and Indole Atoms

atom	gas phase	solution
indole	0.0779	0.2336
C_1	−0.1073	−0.0701
C_2	0.2553	0.2206
N_3	0.2526	0.3759
C_4	0.2095	−0.2933
C_5	−0.3477	−0.0750
N_6	0.1774	0.2283
C_7	0.2036	0.2200
O_8	−0.3471	−0.4322
O_9	−0.3534	−0.4418
C_{10}	−0.0210	0.0343

charges of hydrogens are also summed up to the heavy atoms they are connected. The results from the gas phase and solution data for the basis set 6-311++(d, p) are given in Table 2.

There are several changes detected from this table. First, in the gas phase, the indole ring is relatively neutral, and C_5 is the most negative center. Upon solvation, there is a charge donation from the indole ring to the backbone where a large portion goes to the α carbon. Similarly, there is transfer of 0.25 electrons from C_5 to the backbone.

4. Discussion

First, we compare the results of DFT calculations in the gas and solution phases with native state conformations of the tryptophan in the interest of seeing whether the native conformation introduces new torsional states. The values of ϕ-ψ angles of the torsion angles of tryptophan obtained by the present DFT calculations are shown in Figure 8a by the large filled and empty circles, for the gas and solution cases, respectively. Corresponding values in native proteins are shown in the same figure by the small empty circles. The native state points are calculated using the Protein Data Bank, PDBSELECT,[21,22] which is a subset of the structures in the full PDB[23] that does not contain (highly) homologous sequences. The PDBSELECT contains 1771 chains with 297372 residues. We used 1647 of the chains whose structures were unambiguously defined. There were 4129 tryptophans in these chains, which we used in our statistics.

The sets of large empty and filled circles are the 23 points given in Table 1, each corresponding to low-energy configurations. In Figure 8b, the possible regions allowed for the ϕ-ψ pair are indicated.[24] These regions are separated by steric barriers. The regions indicated in this figure are as follows: α_R, α_L, right and left-handed α-helix regions; β_S, region largely involved in β sheet formation; β_P, extended polyproline-like helices; γ and γ', regions forming tight turns known as γ and inverse-γ turns; δ_R, right-handed region commonly referred to as the bridge region; δ_L mirror image of δ_R region; ϵ, extensive region with $\phi > 0$, $\psi = 180$ that is predominantly observed for Gly; ϵ', mirror image of the ϵ region.

In native proteins, as can be seen from the small empty circles in Figure 8-a, Trp conformations have strong preferences for the β sheet, and right-handed helix regions. The right-handed helix region is joined to the bridge region, which is also densely populated. The inverse turn region γ' is also populated by the native Trp. The left-handed helix region is only sparsely populated. The tight turn region γ is not populated at all. The probability results given in Table 1 and represented by the large circles in the figure show that the lowest energy conformation for the gas-phase calculations is located in the inverse tight turn region, whereas for the solution-phase it is in the β region. The second and third most probable conformations from the gas-phase results are in the β and inverse tight turn regions, respectively. The five most probable configurations for the solution-phase calculations are all in the β region. There is one solution-phase minimum in the right-handed helix region and one in the γ region. The gas-phase results do not yield minima in these two regions.

Conformations indicated by the results of calculations in Figure 8a fall into two categories: (i) Conformations that contain a hydrogen bond among the backbone CO of acetyl and the NH of the amide groups, and (ii) those that lack a hydrogen bond. The hydrogen-bonded structures are the C7 structures making a seven-membered ring, and are those numbered as 6, 11, 12, 20, 21, 22, 23 in the first column of Table 1. Structure 11 in this group lies close to the tight turn region, as may be verified from Figure 8a. The remaining six conformations are all in the inverse tight turn region. The tight turn and the inverse tight turn structures 11 and 21 are shown in Figure 9. The hydrogen bond is indicated with the dotted line. (ii) The remaining structures in Table 1 are those without intramolecular hydrogen bonds, and majority of these are the ones that belong to the low energy β or C5 class.

In the absence of hydrogen bonding, results of DFT calculations represent the intrinsic properties of Trp. Intrinsic energies are those obtained by the conformations of the residue itself. If a Trp is indicated as the ith residue along the peptide chain, the hydrogen bond between the CO of Ace and NH of Nme corresponds to a hydrogen bond between residues $i - 1$ and i. Thus, this hydrogen bond is external to Trp and therefore the calculated energies in the presence of this hydrogen bond are not the intrinsic energies. Thus, only the 16 configurations without the hydrogen bond shown in Table 1 reflect the intrinsic properties of the isolated Trp. The presence of several minima in the right-handed helix region indicates that Trp has an intrinsic tendency to be in helical configuration. In native proteins, helices are stabilized by hydrogen bonds between residues i and $i + 4$. In the present calculations, we obtain minima for the helix state even though the i, $i + 4$ hydrogen bonding does not exist.

Visual examination of the conformations indicates that the indole ring remains as far away as possible from the backbone atoms. In none of the minima, a side group NH forms a hydrogen bond with a backbone CO. Side group conformations are presented in Figure 10. The small empty circles are obtained

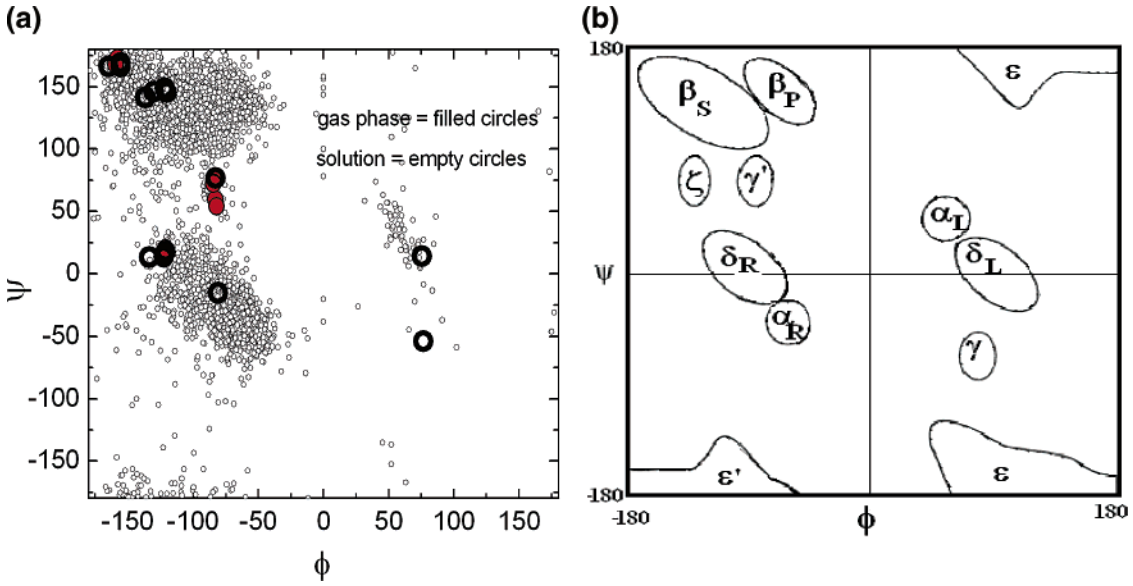

Figure 8. (a) Results of DFT calculations in the gas (filled circles) and solution (empty circles) phases, superposed on native (small circles) states of Trp, and (b) 11 commonly observed states for the 20 amino acids in native proteins.

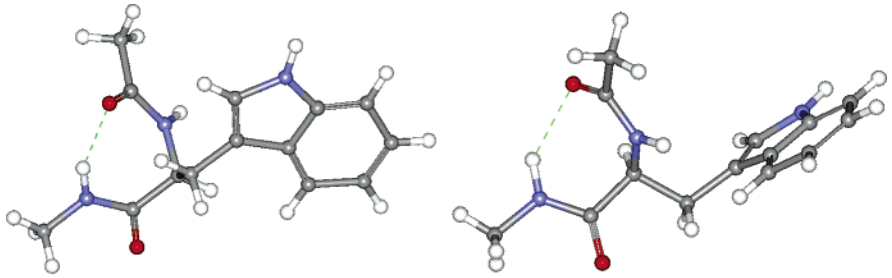

Figure 9. The hydrogen-bonded tight turn (a) and inverse tight turn (b) conformations.

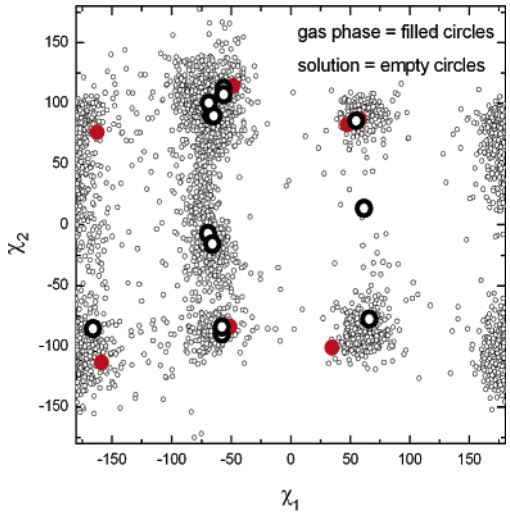

Figure 10. Side group conformations, calculated and native state.

from the native structures. The large filled circles represent gas-phase calculations, and the large empty circles are for the solution structures. Calculated minima fall into highly populated regions in this map. There is only one relatively high-energy structure with $\chi_1 = 62°$ and $\chi_1 = 13°$ that falls into an unpopulated region. With the exception of this minimum, conformations calculated by DFT and reported in Table 1 lie in regions that are highly populated in the native state.

We have also carried out calculations of the solvent effect with IPCM (25). In this formalism, the cavity is formed from isodensity contours. The single point energies of all conformers are calculated both by 6-31g(d) and 6-311++g(d,p) basis sets. In each basis set a different conformer is found to be the global minimum. They are in inverse gamma turn (tight turn) and extended polyproline-like helix region, respectively. However, surprisingly at room temperature all other conformers have almost zero Boltzmann population. This is in strong contrast to the experimental findings summarized in Figure 8.

On the basis of the results of the present calculations, we conclude that, with two exceptions, the single residue DFT calculations yield minima that correspond to the populated regions of the native state. The solution-phase results identify the β region as the most probable state with respect to which the statistical weights of the other states are defined. The present work may be extended to the analysis of neighbor dependence and the perturbation of the potential energy surface resulting from the presence of neighbors.

References and Notes

(1) Daizadeh, I.; Medvedev, E. S.; Stuchebrukhov, A. A. *Proc. Natl. Acad. Sci. U.S.A. Biophys.* **1997**, *94*, 3703.

(2) Dian, B. C.; Longarte, A.; Mercier, S.; Evans, D. E.; Wales, D. J.; Zwier, T. S. *J. Chem. Phys.* **2002**, *117*, 10688.

(3) Huang, Z.; Lin, Z. *J. Phys. Chem. A* **2005**, *109*, 2656.

(4) Compagnon, I.; Hagemeister, F. C.; Antoine, R.; Rayane, D.; Broyer, M.; Dugourd, P.; Hudgins, R. R.; Jarrold, M. F. *J. Am. Chem. Soc.* **2001**, *123*, 8440.

(5) Bombasaro, J. A.; Rodrigues, A. M.; Enriz, R. D. *THEOCHEM* **2005**, *724*, 173.

(6) Jha, A. K.; Colubri, A.; Freed, K. F.; Sosnick, T. *Proc. Natl Acad. Sci. U.S.A.* **2005**, *102*, 13099.

(7) Jha, A. K.; Colubri, A.; Zaman, M. H.; Koide, S.; Sosnick, T. R.; Freed, K. F. *Biochemistry* **2005**, *44*, 9691.

(8) Zaman, M. H.; Shen, M. Y.; Berry, R. S.; Freed, K. F.; Sosnick, T. R. *J. Mol. Biol*. **2003**, *331*, 693.
(9) O'Connell, T. M.; Wang, L.; Tropsha, A.; Hermans, J. *Proteins: Struct. Funct. Genet.* **1999**, *36*, 407.
(10) Avbelj, F.; Grdadolnik, S. G.; Grdadolnik, J.; Baldwin, R. L. *Proc. Natl. Acad. Sci. U.S.A.* **2006**, *103*, 1272−1277.
(11) Hu, H.; Elstner, M.; Hermans, J. *Proteins: Struct. Funct. Genet.* **2003**, *50*, 451.
(12) Mu, Y.; Kosov, D.; Stock, G. *J. Phys. Chem. B* **2003**, *107*, 5064.
(13) Avbelj, F.; Baldwin, R. L. *Proc. Natl. Acad. Sci. U.S.A.* **2004**, *101*, 10967.
(14) Fitzkee, N. C.; Rose, G. D. *J. Mol. Biol.* **2005**, *353*, 873.
(15) Aurora, R.; Rose, G. D. *Protein Sci.* **1998**, *7*, 21.
(16) Frisch, M. J.; Trucks, G. W.; Schlegel, H. B.; Scuseria, G. E.; Robb, M. A.; Cheeseman, J. R.; Montgomery, J. J. A.; Vreven, T.; Kudin, K. N.; Burant, J. C.; Millam, J. M.; Iyengar, S. S.; Tomasi, J.; Barone, V.; Mennucci, B.; Cossi, M.; Scalmani, G.; Rega, N., G. A.; Petersson, G. A.; Nakatsuji, H.; Hada, M.; Ehara, M.; Toyota, K.; Fukuda, R.; Hasegawa, J.; Ishida, M.; Nakajima, T.; Honda, Y.; Kitao, O.; Nakai, H.; Klene, M.; Li, X.; Knox, J. E.; Hratchian, H. P.; Cross, J. B.; Adamo, C.; Jaramillo, J.; Gomperts, R.; Stratmann, R. E.; Yazyev, O.; Austin, A. J.; Cammi, R.; Pomelli, C.; Ochterski, J. W.; Ayala, P. Y.; Morokuma, K.; Voth, G. A.; Salvador, P.; Dannenberg, J. J.; Zakrzewski, V. G.; Dapprich, S.; Daniels, A. D.; Strain, M. C.; Farkas, O.; Malick, D. K.; Rabuck, A. D.; Raghavachari, K.; Foresman, J. B.; Ortiz, J. V.; Cui, Q.; Baboul, A. G.; Clifford, S.; Cioslowski, J.; Stefanov, B. B.; Liu, G.; Liashenko, A.; Piskorz, P.; Komaromi, I.; Martin, R. L.; Fox, D. J.; Keith, T.; Al-Laham, M. A.; Peng, C. Y.; Nanayakkara, A.; Challacombe, M.; Gill, P. M. W.; Johnson, B.; Chen, W.; Wong, M. W.; Gonzalez, C.; Pople, J. A. *Gaussian03*, version B.05; Gaussian Inc.: Pittsburgh PA, 2003.
(17) Becke, A. D. *J. Chem. Phys.* **1996**, *104*, 1040.
(18) Cossi, M.; Scalmani, G.; Rega, N.; Barone, V. *J. Chem. Phys.* **2002**, *117*, 43.
(19) Mennuci, B.; Tomasi, J. *J. Chem. Phys.* **1997**, *106*, 5151.
(20) Miertus, S.; Scrocco, E.; Tomasi, J. *Chem. Phys* **1981**, *55*, 117.
(21) Hobohm, U.; Scharf, M.; Schneider, R.; Sander, C. *Protein Sci.* **1992**, *1*, 409.
(22) Hobohm, U.; Sander, C. *Protein Sci.* **1994**, *3*, 522.
(23) Berman, H. M.; Westbrook, J.; Feng, Z.; Gilliland, G.; Bhat, T. N.; Weissig, H.; Shindyalov, I. N.; Bourne, P. E. *Nucleic Acids Res.* **2000**, *28*, 235.
(24) Karplus, P. A. *Protein Sci.* **1996**, 1406.